Breathing-based Continuous Non-intrusive User Verification Leveraging Commodity WiFi

Huan Dai, Jingjing Jiang, Jiaju Ma, He Huang, and Hongbo Liu

***Abstract*—This paper opens up a new pathway of the utility of breathing pattern for user verification. We demonstrate that it is possible to capture people's breathing pattern leveraging commodity WiFi devices. While prior solutions for biometrics-based user recognition usually require dedicated devices (e.g., video cameras or IR sensors), this paper introduces the first general, low-cost breathing-based user verification system using commodity WiFi devices. The proposed system is based on the fact that the breathing pattern always keeps consistent for the same user but distinct among different people. Our innovative method successfully extracts the breathing pattern of different people based on channel state information of WiFi signal to facilitate user verification. The prototype study using two commodity WiFi devices can differentiate people with an average verification accuracy over 90%, suggesting that our breathing-based user verification system using commerical off-the-shelf (COTS) WiFi is promising to be one of the most critical methods in biometrics.**

***Index Terms*—Breathing pattern, channel state information, security monitoring, user verification.**

I. Introduction

THE rapid evolution of Internet of things (IoT) technologies has led to the provision of versatile ubiquitous network applications and services embedded with modern sensors and intelligent devices (e.g. smart health [1], smart home [2], public safety [3]). In the meanwhile, security issues, especially user verification, become critical for the expansion of IoT [4] as any device is prone to targeted attacks. Comparing with traditional user verification solutions, which require users to memorize and maintain complex passcode, the past decade has witnessed the proliferation of user verification leveraging multiform bio-tokens (e.g., face, fingerprint, iris and gait, etc. [5]–[7]). However, the existing solutions usually rely on specialized equipment or active user involvement. Though popular, these methods either incur extra cost on equipment purchasing and maintenance, or impose heavy burden on bio-token collection at a high frequency for the user to gain continuous access. Continuous verification aims to identify permanently and periodically but not only at a given moment, which provides several advantages like, for example, improve the level of security and the quality of user experience during interaction with applications that require authentication. Therefore, alternative solutions of contact-free, easy deployment, low-cost and continuous biometric recognition would be highly appealing to alleviate the imposition onto the users and provide enhanced security.

In this work, we target continuous non-intrusive user verification for the IoT-based environment. Towards this end, we find that breathing rate, which is a major indicator of a person's vital signs, can serve as a good biometric feature to facilitate continuous non-intrusive user verification [8], [9]. Specifically, the breath of an individual always maintains a steady rate (i.e., 12–20 bpm) and chest motion pattern (i.e., amplitude and variation trend), while different people induce different motion patterns of chest. Therefore, the breathing pattern can be utilized to uniquely determine the user's identity through comparing the measured pattern with previously collected one.

There have been great efforts devoted to related studies on human breath monitoring from both industry and academia. Traditional methods on human breath monitoring rely on hospitalization or wearable devices, which are inconvenient and incur extra cost [10]–[12]. Unlike these methods, radio-based monitoring systems, which exploit wireless signals to capture breathing-induced chest movement, recently attract extensive research interest. In particular, Vital-Radio [13] and WiTrack [14] remotely monitor human breath through capturing the reflected low-power wireless signal of human body with frequency modulated continuous wave (FMCW) radar, which requires a custom hardware with a large bandwidth from 5.46 GHz to 7.25 GHz. Doppler radar [15] and ultra-wideband radar [16] are also adopted to detect human breathing. However, they would continuously occupy a wide band and may impose interference on other devices that share the same spectrum.

Many researchers then resort to commodity devices to perform human breathing monitoring. N. Patwari *et al.* [17] explore using received signal strength (RSS) on the wireless links between commercial wireless devices to estimate human breathing rate. UbiBreath [18] can even detect apnea based on WiFi RSS measurements. The mm-Vital system [19] utilizes the RSS of 60 GHz millimeter wave signals to estimate breathing rates with a larger bandwidth around 7 GHz, but RSS measurements provide coarse-grained channel information, which can only help to derive the breathing rate, and is easy to be affected by ambient interferences. Recently, channel state information (CSI) has been widely adopted to facili-

Manuscript received January 6, 2021; revised Octobor 21, 2021; approved for publication by Klaus Witrisal, Division II Editor, March 2, 2022.

H. Dai, J. Jiang, J. Ma, are with the Department of Electrical and Information Engineering, Suzhou University of Science and Technology, SuZhou215000, China, and Jiangsu Key Laboratory of Intelligent Building Energy Efficiency, SuZhou University of Science and Technology, China, e-mail: {daihuanjob, jiangjingjingsk, majiajujob}@163.com.

H. Huang is with the School of Computer Science and Technology, Soochow University, Suzhou215000, China, email: 2985197044@qq.com.

H. Liu is with the School of Computer Science and Technology, University of Electronic Science and Technology of China, Chengdu, China, e-mail: 653107946@qq.com.

H. Dai is the corresponding author.

Digital Object Identifier: 10.23919/JCN.2022.000011

1229-2370/22/$10.00 © 2022 KICS

tate many wireless sensing capabilities, such as suspicious object detection, indoor localization [20], fall detection [21], human activity recogniztion [22], and RF imaging [23]. It can provide fine-grained channel information with multiple OFDM subcarriers of 802.11n WiFi systems, and is readily available on many commercial WiFi network interface cards (NIC), e.g., Intel WiFi Link 5300 NIC [24] and the Atheros AR9380/9390, AR9580/9590 chipset [25]. Intel 5300 NIC tool only provides CSI for 30 out of the 56 subcarriers, while OpenWrt can capture the CSI measurements from regular data frames [22] which can report CSI data on all the 114 subcarriers. Compared with RSS in MAC layer, CSI depicts fine-grained physical layer information and is more sensitive to environments changes, which makes it more suitable to detect human breathing. S. Lee *et al.* [26] propose a new method for identifying the changes in breathing and heart rate pattern of a person using commercial WiFi devices. Ten participants were evaluated. The accuracy of this method is 94%. J Zhang *et al.* [27] track the human breath using phase variation of CSI. The system Breath track utilizes the hardware correction to calibrate the time-invariant PPL phase offset using cables and splitters. The detailed breath status and the breath rate are extracted by the phase variation of the complex attenuation coefficient. J. Liu *et al.* [28] propose to track vital signs of both breathing rate and heart rate by making use of channel state information in both time and frequency domain during sleep. In both cases, breathing rate is captured by CSI while the raido frequency signal is reflected from the chest of one user, however the breathing pattern difference between different people is not analyzed, and the multi-carrier CSI mining is not sufficient.

In this work, we develop a non-intrusive and continuous user verification system based on people's breathing pattern. The basic idea is to infer people's breath patterns from the fine-grained CSI information, which is collected with commodity WiFi devices, and to verify their identities by comparing with pre-collected breathing pattern profiles. The advantages of the proposed system are two-fold: 1) Our system could be easily applied to existing COTS WiFi devices without introducing extra cost, and 2) our system relies on people's breathing pattern to perform user verification, which is non-intrusive to user's normal behavior, and can achieve continuous verification in practical scenarios. Furthermore, we also upgrade the Atheros CSI Tool and implement the proposed system by developing a new OpenWrt platform, which can obtain CSI data on all the 114 subcarriers on each TX-RX pair. The main contributions are summarized as follows:

- We demonstrate that CSI collected from commodity WiFi can be utilized to verify user's identify. Like user verification with fingerprinting or face, this system can guarantee security with the specificity of everyone's breathing pattern. In particular, it does not require any extra cost compared with the former two systems. To our best knowledge, this is the first work to perform user verification based on breathing pattern with the readily available CSI information from COTS WiFi devices.
- We use CSI phase difference data of the same subcarrier between two different receiving antennas, and develop a novel data extraction method that can precisely separate the breathing measurements caused by chest vibration from the continuous background noise impacted by environments, and extract the breathing pattern which is contained in multi-carrier. Meanwhile, we also build a hyperplane between each classifier upon the breathing pattern.
- Based on CSI tool [29], we upgrade the Atheros CSI tool and develop a new OpenWrt based firmware for TP-link 4900v2, so that the CSI measurements can be collected directly from WiFi routers instead of using laptop or PC with external WiFi NIC adapter. Moreover, our platform can report CSI data on all 56/114 subcarriers over 20/40 MHz channel on each TX-RX pair, which contain more fine-graind information than existing platforms.
- Extensive experiments involving 16 volunteers are conducted under different scenarios. The evaluation results show that our system can achieve over 90% accuracy and thereby validate the effectiveness of the proposed system.

II. Preliminaries & Feasibility Study

A. Channel State Information and MIMO

The CSI represents the channel frequency response (CFR) across multiple orthogonal frequency division multiplexing (OFDM) subcarriers between transmitting antenna and receiving antenna. OFDM, as a multi-carrier modulation technology, divides the wireless channel into a number of orthogonal subchannels, and nowadays is widely applied to many wireless network standards, such as IEEE 802.11n. It can not only weaken the influence of multipath interference, but also greatly reduce inter-channel interference due to the orthogonal channel design. Leveraging the device driver for wireless NICs (e.g, Intel 5300, Atheros Atheros AR9380/9390, AR9580/9590 chipset), the CSI across different OFDM subcarriers can be obtained from each wireless packet to reveal fine-grained wireless physical layer information.

We develop a new OpenWrt platform built upon commodity WiFi router, which can report CSI data across all 56/114 subcarriers, each taking up 20/40 MHz bandwidth. With respect to each subcarrier, the CSI can be expressed as a complex value including both amplitude and phase:

$$H^k = real^k + j \times imag^k = |H^k| e^{j \angle H^k}, \tag{1}$$

where H^k indicates channel response with the central frequency f_k. $real^k$ and $imag^k$ are the in-phase component and quadrature component of k-th subcarrier, $k = 1, 2, \cdots, K$, $K = 56/114$. Respectively, $|H^k|$ and $\angle H^k$ denote the corresponding amplitude and phase of subcarrier k. It describes how the wireless channel is affected by the absorption, reflection and refraction of wireless signal in the surrounding environment, and reveals the multipath effect, shadow fading and distortion between a pair of transceivers.

In radio, multiple-input and multiple-output (MIMO) is a method for multiplying the capacity of a radio link using multiple transmit and receiving antennas to exploit multipath

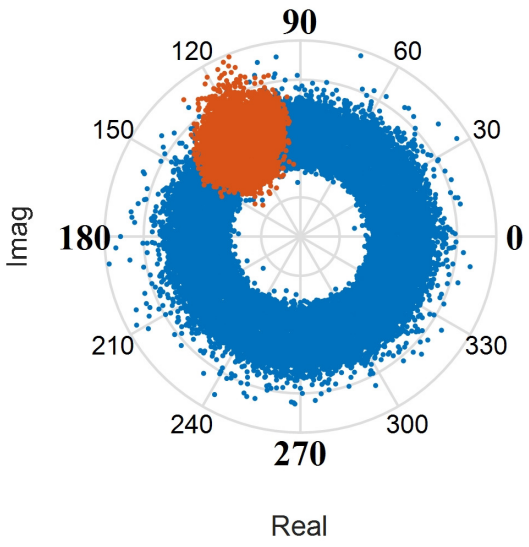

Fig. 1. Comparison between original CSI data (marked as blue points) and the phase difference data (marked as orange points) of the 56-th subcarrier for 20000 consecutively received packets.

propagation. MIMO has become an essential element of wireless communication standards. In 2003, two major competing proposals (TGN Sync and WWISE) agree that the 802.11n standard would be based on MIMO-OFDM with 20 MHz and 40 MHz channel options. For two receiving antennas, the measured CSI phase difference on subcarrier k is stable:

$$\Delta\angle\widehat{H^k_{t_1,r_1r_2}} = \Delta\angle H^k_{t_1,r_1r_2} + \Delta\beta^k_{t_1,r_1r_2} + 2\sigma^2, \quad (2)$$

where $\Delta\angle\widehat{H^k_{t_1,r_1r_2}}$ and $\Delta\angle H^k_{t_1,r_1r_2}$ are the measured phase difference and the true phase difference on subcarrier k between two receiving antennas respectively. $\Delta\beta$ is the unknown phase offset difference, which in a constant due to the phase-locked loop [30], σ^2 is the noise variance.

As shown in Fig. 1, the blue dots represent the raw CSI measurements of 20000 consecutively received packets with respect to the 56-th subcarrier. Phase measured on a single receiving antenna are evenly distributed between $[-\pi\ \pi]$. On the other hand, the red dots denote CSI phase differences between a pair of transceiver antennas. All the phase difference measurements concentrate within two sectors between $\pi/6$ and $5\pi/6$, which clearly indicate that the phase difference is more stable comparing to raw CSI measurements.

B. Breathing Detection

To enable user verification leveraging breathing pattern, it is critical to understand the breathing dynamics first. Breathing includes two phases, inhaling and exhaling, which would cause chest ups and downs in periodic pattern, and the amplitude of chest movement depends on the lung capacity.

According to physiological research [19], the normal breathing rate of adults always maintains at 10-20 breaths per minute (bpm). The chest movement with a certain breathing rate f_b will result in a similar pattern exhibited in the wireless signal reflected from the chest. Specifically, the CSI of any OFDM subcarrier should be a periodic signal of frequency f_k. The CSI phase $\angle H^k$ between a pair of transceivers is:

$$\angle H^k = 2\pi d(t)/\lambda_k, \quad (3)$$

where λ_k is the wavelength of subcarrier k. Given the periodical breathing pattern, the distance becomes:

$$d(t) = D + Acos(2\pi f_b t), \quad (4)$$

where D is the constant mean propagation distance between transceivers. $Acos(2\pi f_b t)$ is the changes of equivalent distance caused by the periodical breathing, which indicates the attenuation of wireless signals during transmission. Thus, the reflected signal phase at the subcarrier k is defined as:

$$\angle H^k = 2\pi(D + Acos(2\pi f_b t))/\lambda_k. \quad (5)$$

The measured phase difference is the CSI phase subtraction between two receiving antenna. Thus, the measured phase difference is also defined as:

$$\Delta\angle\widehat{H_{t,r1r2}} = \angle H_{t,r1} - \angle H_{t,r2}. \quad (6)$$

Since the transmission of each subcarrier has different channel fading, the amplitudes of the subcarriers are different in MIMO system. The phase difference is derived based on the phase of the same subcarrier k at two different antennas $r1$ and $r2$. According to the above two equations, the measured phase difference can be inferred as:

$$\Delta\angle\widehat{H_{t,r1r2}} = 2\pi(D_1-D_2)+(A_1-A_2)cos(2\pi f_b t))/\lambda_k. \quad (7)$$

Where D_1 and D_2 are constant values indicating the average propagation distances between the transmitting antenna and two different receiving antennas r1 and r2; A_1 and A_2 are the amplitudes of CSI measurements caused by the respiratory movement at r1 and r2, respectively. According to the (5) and (7), the measured phase difference also keeps the same frequency of breathing signals f_b.

To verify the consistence of breathing pattern from the same person, Dynamic Time Warping, which is capable of measuring the similarity between two signals of different time scales, is adopted to analyze the phase difference of breathing pattern. Figs. 2(a) and 2(b) depict the similarity of phase difference from the same person and different people, respectively. Through extensive testing work, we found that the phase differences from the breathing pattern of the same person are more similar than those from different people as shown in Fig. 2. It suggests that the breathing pattern of the same person is relatively stable and unique among different people.

We also perform case study to examine the abnormal cardiopulmonary rate. The tester first held his breath, and then breathed normally. As shown in Figs. 3 and 4, we can clearly observe that, when the user holds his breath, his breathing curve is relatively stable, when the user breathes quickly, his breathing fluctuates rapidly. However, when the user breathes normally, the breathing curve returns to normal.

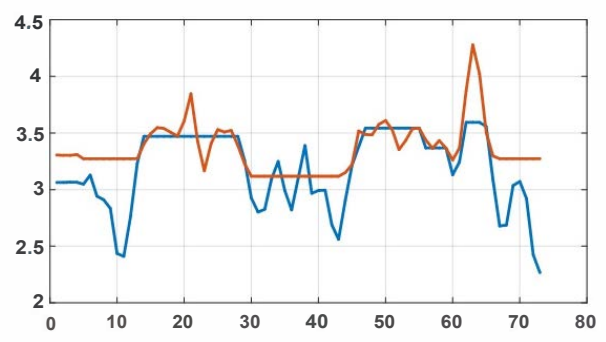

(a) Different users (Cumulative Distance:16.02).

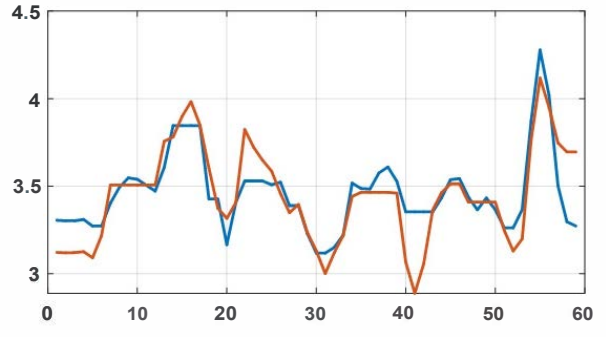

(b) Same user (Cumulative Distance:6.38).

Fig. 2. The performance of DTW represents the uniqueness of user's breathing pattern.

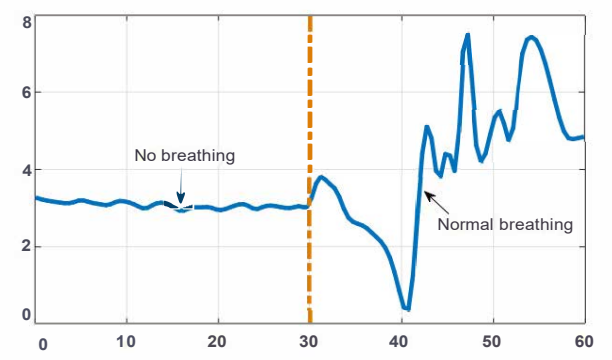

Fig. 3. Different breathing patterns of the same person.

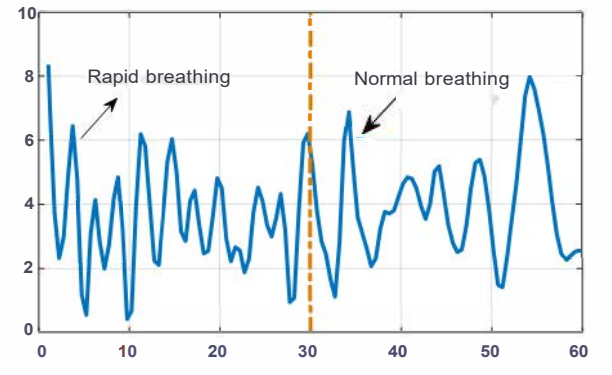

Fig. 4. Different breathing rates of the same person.

III. System Design

A. Challenges

To design a user verification system leveraging user's breathing pattern, the following challenges should be addressed.

Capturing the Breathing Pattern from WiFi Signals Requires Fine-grained CSI. It is non-trivial to obtain such CSI information from commodity devices. Therefore, we need to develop new firmware to collect as much subcarrier information, including both amplitude and phase, as possible.

Resilient to the Environmental Interferences. It is inevitable that the CSI measurements are affected by environmental noise during the user verification process. Sometimes the noise may have comparable intensity as the CSI measurements induced by breathing. Therefore, it is critical to design the system that is resilient to the environmental noise.

Accurate User Verification Leveraging Breathing Pattern. Even with noiseless CSI measurements, it is still a challenging task to achieve accurate user verification with breathing pattern. We first need to extract representative features from CSI measurements to depict the unique breathing pattern for each individual. Such features should be able to capture subtle wireless signal changes caused by user breathing. Given representative features, a suitable classification method should be also developed to accurately identify the legitimate users and reject malicious ones.

B. System Overview

The basic idea of our system is to extract unique user breathing pattern from fine-grained CSI measurements over wireless channel and then verify his/her identity according to pre-defined breathing pattern profiles. Toward this end, we leverage breathing pattern to develop a novel continuous non-intrusive user verification system.

Our system mainly contains three major modules: *Data acquisition*, *breathing feature extraction* and *user verification* which includes training phase and classification phase. As illustrated in Fig. 5, our system first takes the raw CSI measurements as inputs from commodity WiFi devices. Then it conducts breathing rate estimation and breathing feature extraction based on the CSI phase difference after eliminating the DC component and high frequency noises. Then, the SVM based system uses training set to build the hyperplane between each classifier and automatically verifies the user identity in real time.

Data Acquisition. We conduct experiments in three representative indoor environments. The transmitter and receiver are placed next to each other on the table and one user is standing or sitting in the room alone. The commodity devices with our developed firmware implement an OFDM system with 56/114 subcarriers. The collected CSI read from commodity device contain real and imagine values, then reconstruct to H^k.

Breathing Feature Extraction. Based on the collected raw CSI data, this module aims to extract effective biometric features with respect to breathing pattern. Specifically,

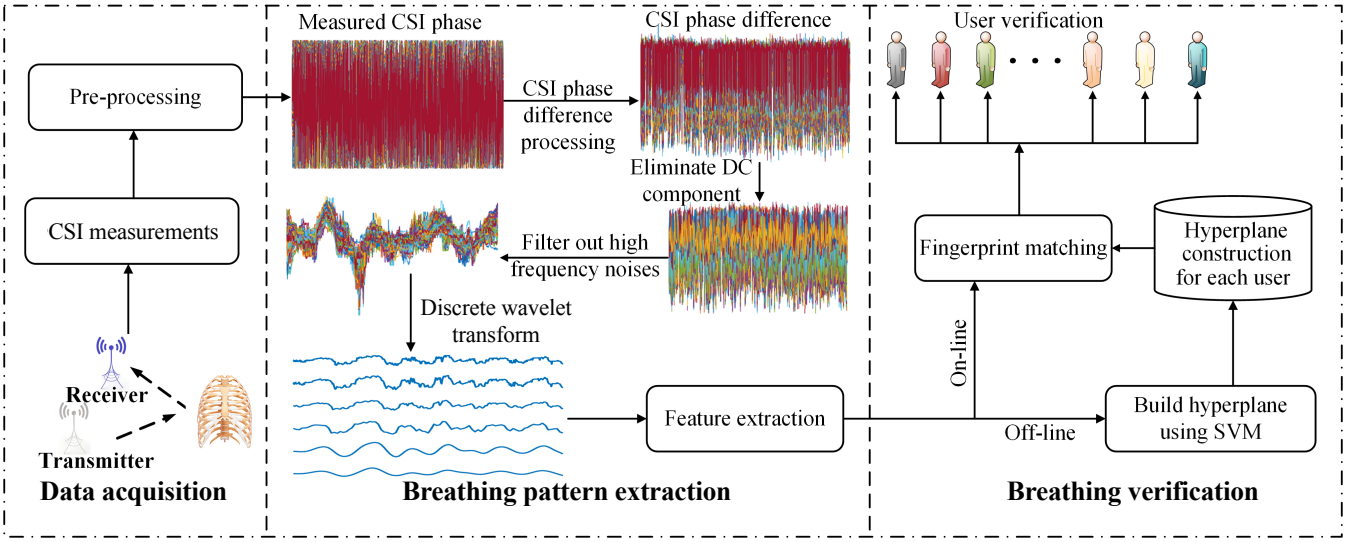

Fig. 5. Overview of the Breathing-based user verification system.

we calculate CSI phase difference to reconstruct the CSI, which depicts the frequency response of each subcarrier in term of phase. Given the reconstructed CSI, our system employs Hampel filter to eliminate the DC component and high frequency noises. Next, discrete wavelet transformation (DWT) is deployed to obtain a time-frequency representation of reconstructed CSI, which are used to extract and select effective breathing features to capture the unique pattern.

User Verification. In this module, we develop a SVM based decision model to verify whether the user is authorized. The result includes three occasions:1) The user is already authorized and the user is allowed to enter the monitored area. 2) the user is not authorized but permitted to be authorized. Thus, we update our model and consider him as the authorized user. 3) the user is not authorized and not permitted to be authorized. The whole authorization mechanism of our system is described as Fig. 5.

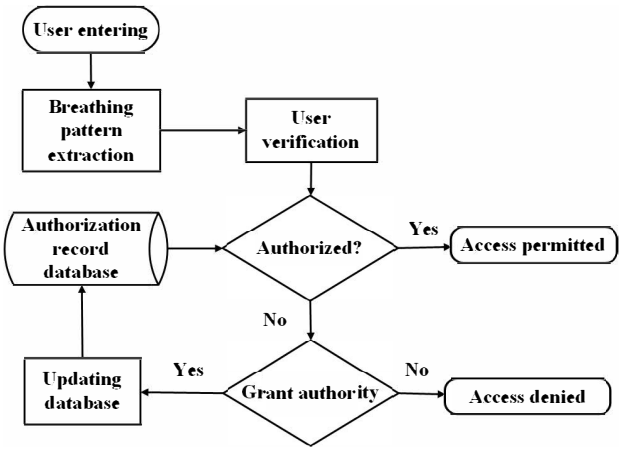

Fig. 6. Security authentication mechanism process.

C. Attack Model

The pattern of attack mainly includes random attack and imitation attack. For the above attacks, our system has mechanisms to mitigate the impact of these attacks and the details are as follows:

Random attack. The attacker does not have any prior knowledge of the user's breathing patterns. When attacking the system, the attacker will stay at the same location as the user does and breathe freely in terms of the breathing rate, inhale/exhale rhythm, and deepness. In response to this attack, when our collecting the CSI data, the person breathes in a randomly chosen style including eupnea, tachypnea and etc. This mechanism greatly improves the robustness of our system, so that we can deal with the random attack efficiently.

Imitation attack. The attacker observes how the user passes the verification and will stay in the same location as the user does and try to mimic the user's breathing pattern. Everyone's chest is unique and the breathing information is not the same as fingerprint and human face which can not be imitated easily. So, in our system, the problem of anyone copying the user's personal characteristics to crack the authentication system can be avoided. Furthermore, breathing based security system provides continuous verification which avoids the problem that the adversary only adopting once attack makes the system broken down. So, our system can solve the imitation attack.

IV. Breathing Pattern Extraction

A. Data Acquisition

In wireless environment, when the person inhales and exhales, his/her chest expands and contracts, which will affect the wireless signals. However, wireless signal transmission usually experiences various environmental impacts (e.g., absorption, reflection, refraction), resulting in unstable raw CSI measurements, which are unfavorable to detect chest motion. The key challenge in breathing signs detection leveraging wireless signals is how to mitigate the environmental impact and any irrelevant motion that affect the raw CSI signals. So,

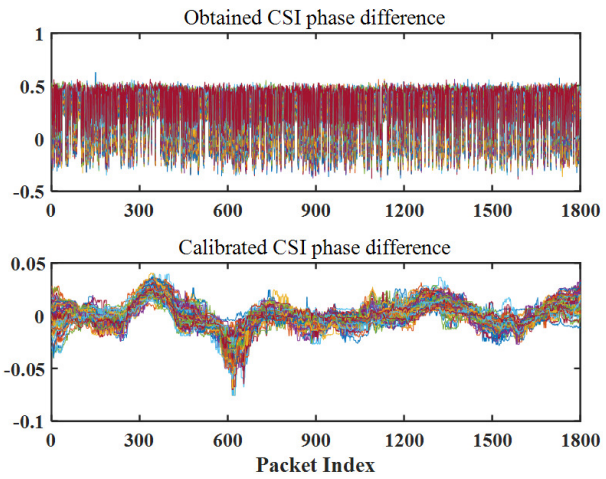

Fig. 7. Comparison between obtained CSI phase difference and calibrated CSI phase difference.

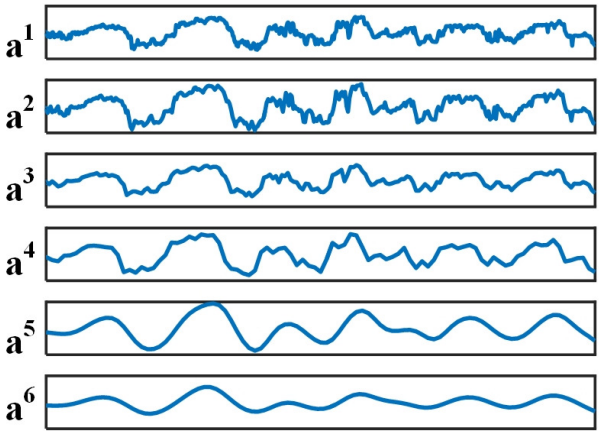

Fig. 8. Transform steps of discrete wavelet transform results.

data preprocessing is essential to facilitate effective breathing pattern detection.

Our preliminary study finds that CSI phase difference data is relatively stable and periodic, and what's more, CSI phase difference data and breathing signal has the same frequency in a stationary environment. As shown in Fig. 5, the weak breathing feature drowns in high frequency noises and DC component, and it is difficult for us to extract the feature. We propose to exploit two Hampel filters to obtain robust CSI phase difference. Specifically, Hampel filter with the sliding window of 300 and the threshold of 0.001 is employed to capture the basic trend of CSI phase difference. To eliminate the DC component, we subtract the basic trend data from the CSI phase difference data. The detrended data is beneficial to preserve as much detail as possible of CSI phase difference. What's more, the Hampel filter is leveraged with a 50 samples sliding window and the same threshold of 0.001 to eliminate high frequency noises.

As illustrated in Fig. 7, the trend of CSI phase difference is preserved after eliminating high frequency noises and the DC component, and the CSI phase difference of each subcarrier appears as a periodic signal over the packets with low noise.

B. Breathing Feature Extraction

The breathing-induced chest motion is a minute and periodic movement, and such periodic pattern can serve representative breathing features. In order to extract such breathing features from CSI phase difference, we explore the efficacy of different frequency domain methods including FFT, short time Fourier transform (STFT) and DWT. Different from FFT and STFT, DWT can not only characterize a time-frequency representation, but also provide a multi-scale resolution of CSI phase difference. In this work, we therefore adopt DWT to capture the periodic breathing signal.

The phase difference $\Delta\angle\widehat{H^k_{t_1,r_1r_2}}(n)$ after data preprocessing, can be decomposed into multiple tiers with wavelet decomposition as follows:

$$\Delta\angle\widehat{H^k_{t_1,r_1r_2}}(n)=\sum_{k\in Z}\mathbf{a}^L_k(n)\phi^L_{n-2^Lk}+\sum_{l=1}^{L}\sum_{k\in Z}\mathbf{d}^l_k(n)\varphi^l_{n-2^lk}, \tag{8}$$

where L is expressed as the number of decomposition tiers. $\mathbf{a}^L$ and $\mathbf{d}^L$ represent approximation coefficient and detail coefficient respectively. $\phi's$ and $\varphi's$ represent wavelet bases. The approximation vector represents the large-scale features of the input signal. The detail vector represents the small-scale features of the input signal and describes the high-frequency noise part of the input signal. We can compute DWT coefficient as follow:

$$\begin{cases}\mathbf{a}^L_k(n)=\sum_{n\in Z}\Delta\angle\widehat{H^k_{t_1,r_1r_2}}(n)\phi^L_{n-2^Lk},\ L\in Z\\ \mathbf{d}^l_k(n)=\sum_{n\in Z}\Delta\angle\widehat{H^k_{t_1,r_1r_2}}(n)\phi^l_{n-2^lk},\ l\in\{1,\cdots,L\},\end{cases} \tag{9}$$

where $\Delta\angle\widehat{H^k_{t_1,r_1r_2}}(n)$ is the adjusted phase data, Z is the integer set, ϕ's and φ's are wavelet basic functions.

In order to find the most appropriate L to approximate coefficient $\mathbf{a}^L$ to detect the breathing rate, the sampling rate is halved after each decomposition until the frequency of $\mathbf{a}^L$ is as close to the breathing rate as possible.

$$\frac{fs}{2^L}\approx Bs, \tag{10}$$

where Bs is the breathing rate ranging from 0.17 Hz to 0.62 Hz, fs is the sampling number of discrete signals extracted from signals per second. As shown in Fig. 8, the measured CSI phase difference has undergone six tiers of DWT, where the noise is suppressed at each tier.

As shown in Fig. 8, $\mathbf{a}^6$ becomes a periodically denoised signal over packets. We compute the breathing rate with the average peak to peak intervals according to local peak identification and breathing cycles combination. The breathing rate in Fig. 9 is approximately 0.22 Hz, which is excatly the same as the breathing rate acquired by respiration monitor Glory tls-b19 Watch. It reflects that $\mathbf{a}^6$ characterizes breathing features.

Next, the breathing information which extracted using DWT is short-term data and the characteristics of the periodicity

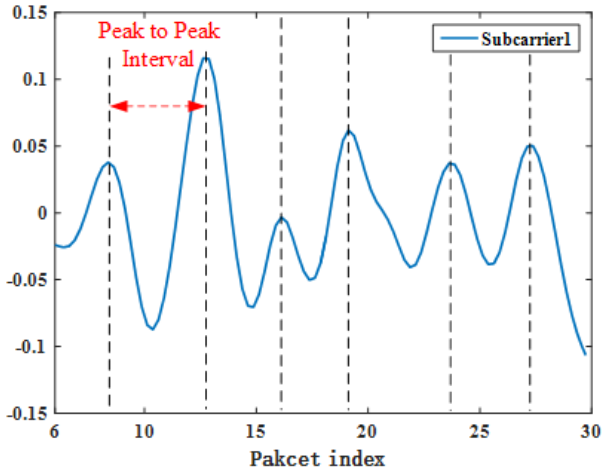

Fig. 9. Breathing patterns of individual users (standing and facing the device).

Algorithm 1: Breathing features extraction

Input: CSI data **H** of 56/114 subcarriers

Output: the characteristics of the periodicity of breathing

For each subcarrier CSI $H^k \in$ **H do**

1. Data Preprocessing

-Calculate the CSI phase difference $\Delta\angle H^K$:

$\Delta\angle\widehat{H^k_{t_1,r_1r_2}} = \Delta\angle H^k_{t_1,r_1r_2} + \Delta\beta^k_{t_1,r_1r_2} + 2\sigma^2$

2. Filtering redundant information

-Hampeling CSI phase difference data

-Compute DWT coefficient $\mathbf{a}^L$:

$\mathbf{a}^L_k(n) = \sum_{n\in Z} \Delta\angle\widehat{H^k_{t_1,r_1r_2}}(n)\phi^L_{n-2^Lk}$

End

3. Calculating results

-Obtain the feature of breathing pattern $\hat{\mathbf{A}}(n)$:

$\hat{\mathbf{A}}(n) = \{\mathbf{A}(n)\ \mathbf{A}(n+1)\cdots\mathbf{A}(n+T-1)\}$

of breathing should be composed of several short-term data. Thus, in this study, we adopt a kind of matrix transformation to capture and preserve the periodicity of breathing from the breathing information. In particular, assuming that we would like to explore this method to ascend the i-th short-term data of y-th person $\mathbf{A}(n)$ to $\hat{\mathbf{A}}(n)$ and the formula of the matrix transformation is as follows.

$$\hat{\mathbf{A}}(n) = \{\mathbf{A}(n)\ \mathbf{A}(n+1)\cdots\mathbf{A}(n+T-1)\}, \qquad (11)$$

where $n = 1, 2, \cdots, N$, N is the quantity of breathing information sample data, $\mathbf{A}(n) = \{\mathbf{a}_1(n)\ \mathbf{a}_2(n)\cdots\mathbf{a}_K(n)\}$ is vector of breathing information which mentioned in section 4.2, K is the number of subcarriers, T denotes the length of duration. $\hat{\mathbf{A}}(n)$ is the features which are used to train model for verify the user identity. Through this kind of matrix transformation, each sample can cover the entire respiratory process. What's more, this method reduces training samples without reducing the total amount of data. It will reduce training time complexity and greatly improve training efficiency. As demonstrated in Algorithm 1, the algorithm of breathing feature extraction works in three procedures: 1) Data Preprocessing, 2) filtering redundant information and 3) breathing feature extraction.

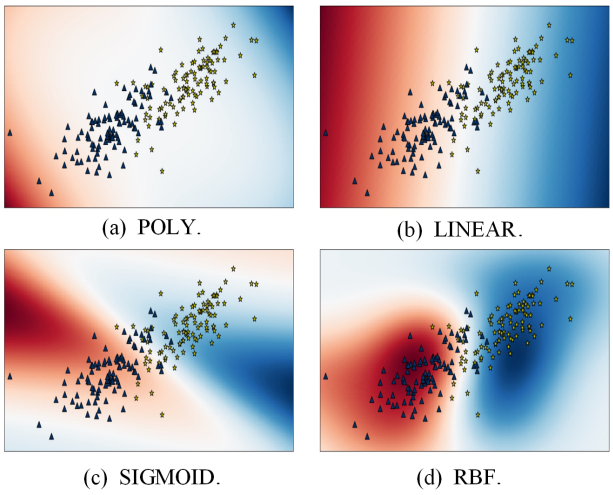

Fig. 10. The performance of different kernel function.

V. Breathing Verification

In this section, we explore representative breathing features that could facilitate human identity verification and build SVM classifier using kernel function.

A. Kernel Function Selection

In our system, kernel function is applied to map the original sample space to a higher dimensional feature space. By using the kernel function, SVM based classification is able to find a hyperplane in a high dimensional space. It solves the problem of complex computation of data in low-dimensional space.

The selected parameter is the best super parameter of SVM kernel. Regularization parameter C = 1, kernel function parameter gamma = 0.01. As described in Fig. 10, pentagons and triangles present the two clusters which are the features of two people. It can be seen that the performance of RBF distinguishing the two categories is obviously superior to that of other three kernel function. Therefore, RBF is adopted to our system to distinguish the user identity. The equation of RBF is as follows:

$$\kappa(\hat{\mathbf{A}}(i), \hat{\mathbf{A}}(j)) = \exp(-\frac{||\hat{\mathbf{A}}(i) - \hat{\mathbf{A}}(j)||^2}{2\delta^2}), \qquad (12)$$

where δ is the width of the RBF, $\hat{\mathbf{A}}(i)$, $\hat{\mathbf{A}}(j)$ denote two breathing pattern samples.

B. SVM-based Classification

The training model for SVM classifier is to establish the functional dependency between breathing feature $\hat{\mathbf{A}}(n)$ and user identity y. Assume l denotes the feature dimension and N is the number of labeled samples in the training set. Each labeled sample consists of a pair $(\hat{\mathbf{A}}(n), y), n = 1, \cdots, N$, where $\hat{\mathbf{A}}(n)$ is a vector representing breathing information, y denotes the serial number of users. The training model seeks for a hyperplane to distinguish between categories using

TABLE I
DEVICE PARAMETERS.

Symbol	Value	Description
N_{rx}	3	The number of transmitting antennas in MIMO Control field.
N_{tx}	3	The number of receiving antennas in MIMO Control field.
Ns	56/114	The number of subcarriers the routers sent.
fs	60 Hz	The sampling number of discrete signals extracted from continuous signals per second is defined, which is expressed in Hertz (Hz). The reciprocal of sampling frequency is the sampling period or sampling time, which is the time interval between samples.
BW	20/40 MHz	Refers to the amount of data that can be transmitted at a fixed time, that is, the ability to transmit data in a transmission pipeline. Usually expressed as a transmission cycle per second or Hertz (Hz).

the empirical dataset $\{(\hat{\mathbf{A}}(n), y)|n = 1, 2, \cdots, N\}$ and the calculation formula is as follows:

$$\begin{cases} \max_{\alpha} \sum_{i=1}^{N} \alpha_i - \frac{1}{2} \sum_{i=1}^{N} \sum_{j=1}^{N} \alpha_i \alpha_j y_i y_j \kappa(\hat{\mathbf{A}}(i), \hat{\mathbf{A}}(j)) \\ s.t. \sum_{i=1}^{N} \alpha_i y_i = 0, \alpha \geq 0, i = 1, \cdots, N \end{cases}, \tag{13}$$

where the α is the Lagrange multiplier, κ is the kernel function mentioned above, y_i and y_j represent the user identity of $\hat{\mathbf{A}}(i)$ and $\hat{\mathbf{A}}(j)$. Solving above equation, we can get decision function to determine prediction result:

$$f(\hat{\mathbf{A}}) = \mathbf{sgn}(\sum_{i=1}^{N} \alpha_n y_i \kappa(\hat{\mathbf{A}}(i), \hat{\mathbf{A}}) + b), \tag{14}$$

where **sgn** returns the positive and negative sign of the predicted result and the positive sign represents the prediction results of respiratory information and identity sequence classification, b is the offset of the hyperplane.

VI. Experiment And Evaluation

This section presents the experimental settings and results of our system. Firstly, we describe the experimental environment and data acquisition methods. Then, we demonstrate the impact of the number of subcarriers, the number of antennas and some other parameters on the identity verification accuracy. Finally, we also compare the result of different users to explore the robustness of our system.

A. Experimental Methodology

To validate the proposed user verification system, we deploy two TP-link 4900v2 wireless routers: one severs as transmitting antenna and the other as receving antenna. Meanwhile, we developed a new OpenWrt platform implemented on the routers to collect the CSI measurements from regular data frames. In order to obtain less interference and higher distance resolution data, we operated on 5 GHz frequency band. In addition, we leveraged 20/40 MHz channel bandwidth which introduces 56/114 subcarriers to capture more detailed channel information than Intel NIC 5300. All 3 transmitting antennas are used to transmit packets at 60 packets per second to 3 receving antennas. We can capture 3×3×56 CSI streams at each time instant. The detailed parameters are provided in Table 1.

Fig. 11. The experiments scenes and devices.

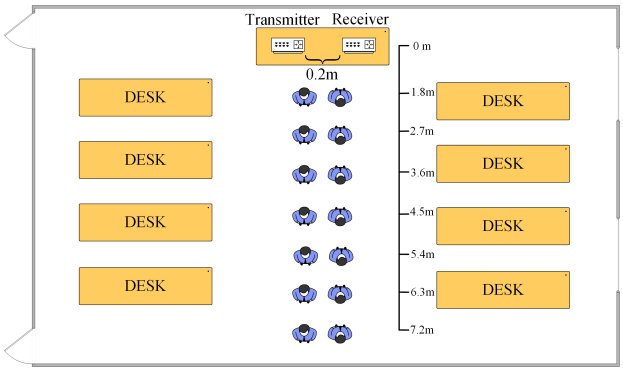

Fig. 12. Experimental setting to verify the influence of distance and human body's orientation.

Experiments were conducted involving 16 volunteers. The

TABLE II
CHARACTERISTICS OF VOLUNTEERS.

	A	**B**	**C**	**D**	**E**	**F**	**G**	**H**
Gender	M	M	M	M	M	M	M	M
Age	25	24	27	25	19	21	31	35
Height (cm)	183	180	172	177	180	178	184	165
Weight (kg)	76	70	78	76	68	72	80	75
	I	**J**	**K**	**L**	**M**	**N**	**O**	**P**
Gender	F	F	F	F	F	F	F	F
Age	18	25	19	22	27	20	30	29
Height (cm)	160	158	160	169	155	159	161	166
Weight (kg)	47	44	51	55	57	41	59	57

TABLE III
ACCURACY OF DIFFERENT ALGORITHMS.

Algorithms	$K = 36$, $T = 30$		$K = 56$, $T = 60$	
	Accuracy	S.D.	Accuracy	S.D.
KNN	73.9%	2.31	78.9%	1.89
RF	81.4%	0.55	84.4%	0.46
ANN	90.6%	0.32	93.6%	0.11
SVM	94.7%	0.78	96.7%	0.54

TABLE IV
COMPARISON OF BREATHING BASED AUTHENTICATION SYSTEM.

System	**Signal source**	**Feature extraction**	**Accuracy**
[31]	Rader	FFT and Dynamic Segmentation	92.0%
BreatheSec [32]	RF	CNN	95.2%
Our system	CSI	DWT	94.7%

characteristics of volunteers are shown in Table 2. The experiments scenarios include an office room (6 m×10 m), a laboratory(12 m×12 m) and a 26 m long corridor as shown in Fig. 11. The first scenario office room is crowded with various furniture; the second setup is a laboratory scenario, a cluttered environment with tables and metal chairs, and electronic laboratory cases; and the third scenario is a corridor with no other objects except experimental equipment. Fig. 12 demonstrates the floor plan of testing scenario and the locations of TX and RX routers. In our experiments, the two routers are placed side by side on the table, which are 20 cm apart from each other at a height of 70 cm. Every scenario conducted 256 testing rounds which contained 5 experimental variables (e.g., user position, user sitting, user standing, user facing or back to access points). In each round of test, 20000 samples of each testing process performed by one volunteer were collected.

B. Evaluation Metrics

Accuracy. Given n_s testing set, y_i' is the prediction of the i-th sample and y_i is the corresponding groundtruth, then the accuracy of verifying the user's identity y over n_s is defined as:

$$accuracy(y, y') = \frac{1}{n_s} \sum_{i=0}^{n_s-1} 1(y_i' = y_i), \tag{15}$$

where $1(x)$ is indicator function defined as:

$$1_A(x) := \begin{cases} 1 & \text{if } x \in A \\ 0 & \text{if } x \notin A \end{cases}. \tag{16}$$

Misjudgement. Probability of misjudegement indicates the proportion of the number of misjudged individuals in the total. It is defined as:

$$PM(y, y') = \frac{1}{n_s} \sum_{i=0}^{n_s-1} 1(y_i' \neq y_i). \tag{17}$$

C. Impact of Algorithms

Table 3 compares the verification results of four different algorithms. when the number of subcarriers is 36 and T is 30, random forest (RF), 'splitter' which is used to choose the split at each node is 'best') and K-nearest neighbor (KNN) ('leaf_size' which affects the speed of the construction and query is 30, the number of neighbors is 5) which are not applicable to our data has the verficiation accuracy as low as 54.2% and 73.9%. The verification rate of artificial neural network (ANN) is better (i.e., 90.6%) with 3 hidden layers where each has 32 neurons. SVM achieves the best performance with the verification average accuracy of 94.7%.

It can be seen from Table 3 that when $K = 56$, $T = 60$, the accuracy of the algorithm is higher than when $K = 36$, $T = 30$. So the following experiments are based on $K = 56$, $T = 60$.

Table 4 summarizes the respiratory authentication systems based on IoT devices using neural networks. The radar and RF equipment in [31] and [32] require specialized devices with highly complex design, making many users can not affording them, and many public users can't afford it. Our system provides a low-cost, efficient and highly accurate solution with fine-grained CSI measurements.

D. Impact of the Antennas and its direction

Fig. 13(a) shows that different transmitting antenna has different performance on identifying user. The direction and position of antenna both cause the change of accuracy. The parameters of the same type of antenna products have different performance. This is mainly due to the problem of antenna consistency. When the stationary Bobbi curve of an antenna is irregular and disordered, the consistent performance of the antenna is poor. Therefore, in terms of verification accuracy, some antennas will perform poorly. The highest verification accuracy of transmitting antenna1, transmitting antenna 2 and transmitting antenna 3 are 84.7%, 99.1% and 96.7% when the router is vertical to the users and the accuracy is 86.4%, 98.1% and 96.1% when the router is parallel to the users, respectively.

Fig. 13(b) presents the performance of user identity verification with different number of transmitting antennas. When the number of transmitting antenna is 1, 2 and 3, the average

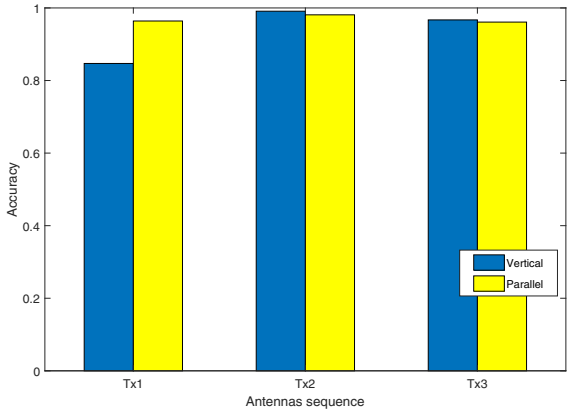

(a) Different antennas.

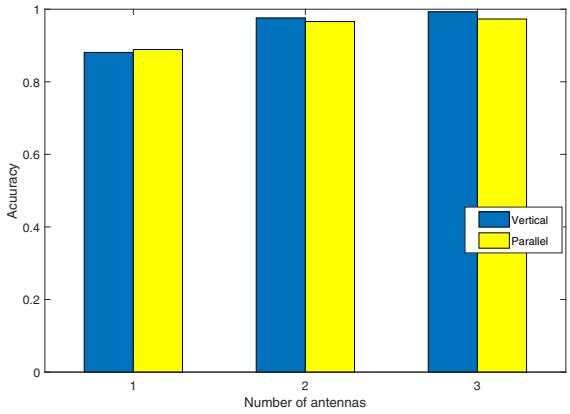

(b) Different number of antennas.

Fig. 13. The performance of antenna in different situations.

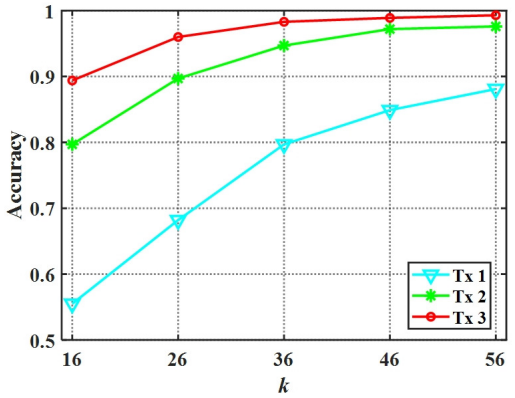

Fig. 14. The performance of different subcarrier number using different antenna.

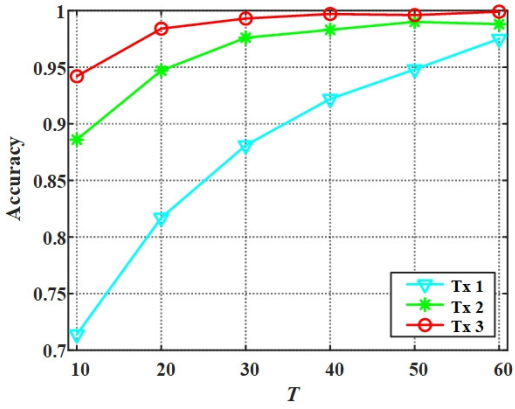

Fig. 15. The performance of parameter T using different antennas.

verification accuracy is 88.1%, 97.6% and 99.3% when the router is vertical to the users and the accuracy is 88.9%, 96.6% and 97.3% when the router is parallel to the users, respectively. Obviously, in MIMO system, the number of transmitting antenna have a significant impact on verification accuracy. Specifically, the highest verification accuracy with multiple antennas is 17% higher than the setting involving single antenna pair, and an additional pair of antennas will increase verification accuracy about 8%. This is because MIMO system can better mitigate the multi-path effects, and more pairs of antennas can accurately capture the breathing dynamics by eliminating the multi-path effects.

E. Impact of The Number of Subcarriers

As shown in Fig. 14, our system with more subcarriers has higher verification accuracy, and it indicate that more subcarriers include richer breathing-related information which are beneficial to identify the users. It is also noticed from Fig. 14 that the effect of subcarrier number on each transmitting antenna is different. For the transmitting antenna 1, the verification accuracy is significantly affected by the number of carriers, i.e. the highest verification accuracy is 36% higher than the lowest one. But the transmitting antenna 2 or the transmitting antenna 3, the effect is subtle, i.e. the highest verification accuracy is only about 8% higher than the lowest one.

F. Impact of Duration of Breathing Cycle

Fig. 15 depicts the effect of parameter T, which indirectly denotes the length of breathing duration on verification accuracy. As indicated in Fig. 15, when the value of T is greater than 50, the accuracy of the system exceeds 95%. In fact, a person's breathing cycle is about 3.5 s, the data frequency is about 15 Hz, the value of parameter T of one duration of breathing cycle is about 52.5 (3.5×15), thus, when the measured signal reaches a breathing cycle, the system can achieve high accuracy.

G. Impact of Human Factor

User's position and orientation also have a great impact on the verification accuracy. Fig. 16 describes the effect of user's position and orientation on average verification accuracy. What's more, when the distance is shorter, the change rate of accuracy is obvious. On the other side, we can see that the average verification accuracy of user back to routers is significantly higher than that of facing routers especially at long distances.

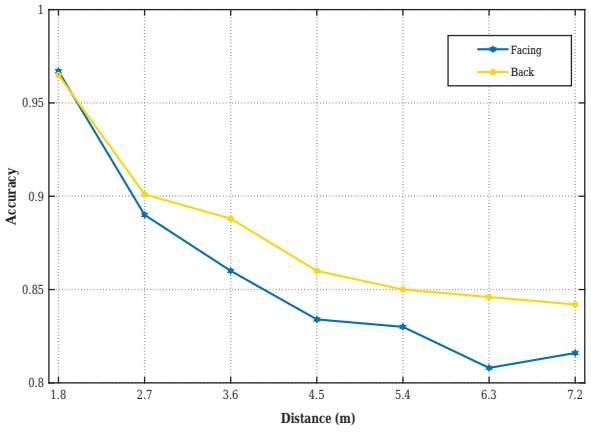

Fig. 16. The performance of user's position and orientation.

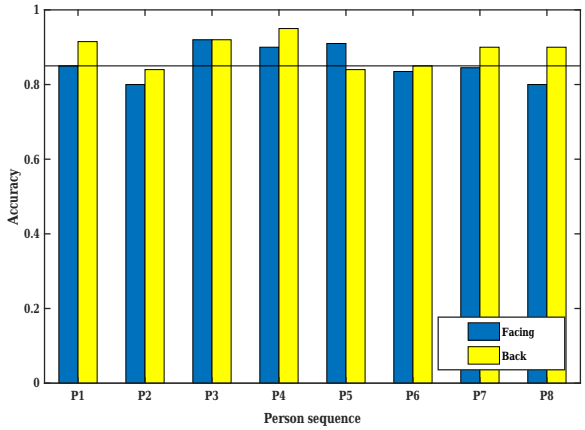

Fig. 18. The performance of different user standing face or back to routers.

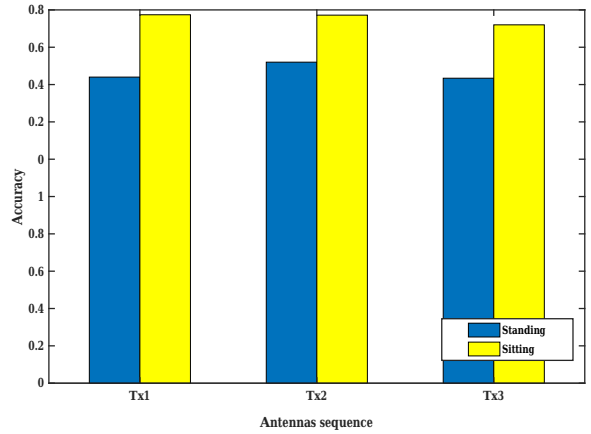

Fig. 17. The performance of user sitting and standing.

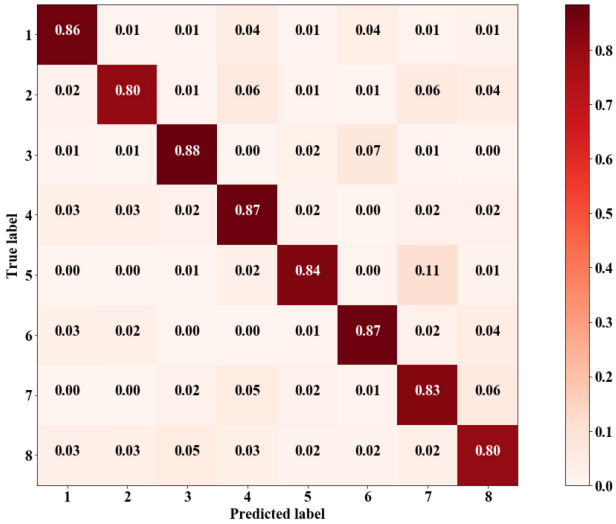

Fig. 19. The confusion matrix of verifying 8 users.

Human posture is another critical impact factor on the verification accuracy. The relatively static motion has stable signal characteristics and chest is closer to router when sitting down. These two reasons leading to higher verification accuracy. We study the performance of the proposed system when user is sitting or standing. Sitting represents a relatively static motion and standing is the opposite. Fig. 17 shows the average verification accuracy with different transmitting antenna, it is encouraging to find that the accuracy of sitting posture (i.e., 96.1%) is obviously superior to that of standing (i.e., 87.1%).

H. Impact of Different Users

mFig. 18 presents the verification accuracy across different persons. Specially, the average verification accuracy of all the users are 81% and 85%, respectively, and the lowest average accuracy among all the participants is still above 80%. The standard deviation of the result is about 0.04. In these experiments, the distance from router to person is 5.4 m, T is 30, the number of transmitting antenna is 3 and the number of subcarriers is 56. The results show the robustness and scalability of our verification system across different users, and demonstrate the system is promising to act as a safety verification system which is suitable to different users.

Fig. 19 shows the confusion matrix of verifying 8 users. The distance from router to person is 5.4 m, T is 30, the number of transmitting antenna is 3 and the number of subcarriers is 56. The average verification accuracy is about 85%. Although there are differences in age, height, weight and gender of eight people, it can be seen from the figure that the probability of misclassification among users is relatively uniform. We can conclude that the difference between people has little effect on our system.

I. Impact of Trainging Data Size

Next we study the performance of our system under different training data size as shown in Fig. 20. In particular, the system achieves an accuracy of 63.7%, 82%, 93%, 97.4%. when choosing 20%, 40%, 60%, 80% of entire training set. We observe that our system can achieve an average precision of over 80% for 8 users with 40% training set. As the size of the training data grows, the system performance improves significantly. The above results indicate our system can achieve good verification performance with a limited size of training

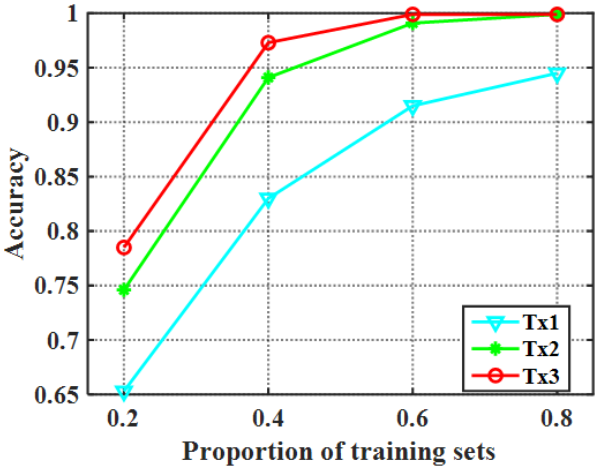

Fig. 20. The performance of proportion of training sets using different antennas.

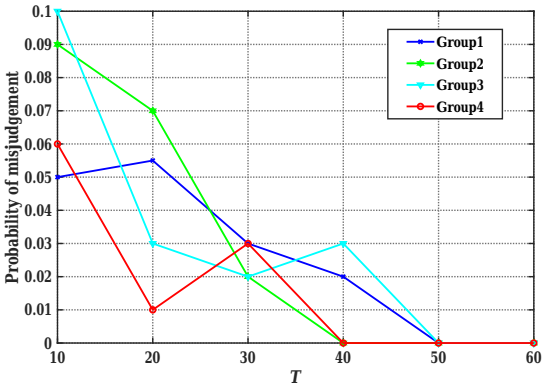

Fig. 21. The performance of attack model with different T.

data, which ensures great convenience for practical usage on commodity WiFi. In these experiments, the distance from router to person is fixed at 5.4 m, T is 30, the number of transmitting antenna is 3 and the number of subcarriers is 56.

J. Immunity to Malicious Attacks

In order to further validate the immunity of the proposed system to imitation attack, we partition the eight users into four groups and ask a user in each group to act as the attacker by imitating the breathing pattern of the other. The imitation attacker aims to bypass our user verification with the imitated breathing pattern of legitimate user. To make the imitation more realistic, the breathing pattern of legitimate user will be recorded for the attacker to imitate. Fig. 21 shows the probability of misclassification for four groups with different T. We can find that the probability of misclassification during the experiment always maintains at a low level (i.e., less than 0.1). Moreover, when T is above 50, all the imitation attacks are correctly identified, indicating the resilience of the proposed system to imitation attack.

VII. Conclusions and Discussion

This paper explores the feasibility of using commodity WiFi for non-intrusive user verification based on breathing pattern. Compared with fingerprinting and face verification, this system does not require any extra cost in terms of hardware. Moreover, it is capable of preventing random and imitation attack with promising continuous verification. Our system have upgraded the Atheros CSI tool and developed a new OpenWrt based firmware, so that the CSI of all 56/114 subcarriers over 20/40 MHz can be aggregated directly from WiFi routers instead of using laptop or PC with external WiFi NIC adapter. The CSI phase difference data between two receiving antennas was first succesfully derived. The breathing measurment cased by chest vibration was then separated from continuous background nosie. Extensive experiments are conducted with 16 objects in different rooms with different positions and different orientations. The impact of the number of antennas and subcarrier was evaluated as well. The results reveal that the proposed system could achieve over 90% accuracy.

Overall, this work proposes a practical and effective WiFi-based user verification system leveraging the unique breathing pattern. To our best knowledge, maybe not the first but still a very valid contribution. We envision that the proposed system can be extensively adopted by many security-critical applications, and contribute to both personal and corporative security services. As the very first trial in this field, our system has also its limitation. Currently our system can achieve high verification accuracy with respect to single user in the area of interest. The presence of multiple people will introduce mutual interferences on extracting breath patterns from WiFi signals, and degrade the performance of our system. Our next step is to build a thorough signal propagation model depicting the relationship between signal variation and multi-user breathing. Furthermore, more complex scenarios, including different user movements and environments, user having cardiopulmonary diseases, will also be taken into consideration to improve the robustness and scalability of the proposed system.

Acknowledgment

The authors would like to thank the National Natural Science Foundation of China (Grant no. 61702354, Grant no. 61876121), the Scientific Research Project of Suzhou University of Science and Technology (Grant no. XKZ2017004), the Key Laboratory of Mobile Interconnection Technology Engineering of Jiangsu Province (Grant no. JSWLW2017004), and the Graduate Research Innovation Project (Grant no. SKSJ18_012, Grant no. SJCX19_0963).

Conflict of interest. The authors declared that they have no conflicts of interest to this work.

References

[1] Y. Gu, J. Shen, and Y. Chen, "Poster abstract: Know you better: A smart watch based health monitoring system," in *Proc.IEEE/ACM CHASE*, 2019, pp. 7–8.

[2] S. K. Sooraj, E. Sundaravel, B. Shreesh, and K. Sireesha, "Iot smart home assistant for physically challenged and elderly people," in *Proc. IEEE ICOSEC*, Sep. 2020, pp. 809–814.

[3] C. Chatzigeorgiou, M. Feidakis, D. G. Kogias, and C. Z. Patrikakis, "Increasing safety and security in public places using iot devices," in *Proc. IEEE WF-IoT*, Jun. 2020, pp. 1–2.
[4] J. Iskander, A. Abobakr, M. Attia, K. Saleh, D. Nahavandi, M. Hossny, and S. Nahavandi, "A k-nn classification based vr user verification using eye movement and ocular biomechanics," in *Proc. IEEE SMC*, vol. 18, Oct. 2019, pp. 1844–1848.
[5] F. Liu, Q. Zhao, X. Liu, and D. Zeng, "Joint face alignment and 3d face reconstruction with application to face recognition," *IEEE Trans. Pattern Anal. Mach. Intell.*, vol. 42, no. 3, pp. 664–678, Mar. 2020.
[6] D. V.-R. *et al.*, "A review of fingerprint feature representations and their applications for latent fingerprint identification: Trends and evaluation," *IEEE Access*, vol. 7, pp. 48 484–48 499, 2019.
[7] W. W. A. *et al.*, "Neurophysiological correlates of gait retraining with real-time visual and auditory feedback," *IEEE Trans. Neural Syst. Rehabil. Eng.*, vol. 27, no. 6, pp. 1341–1349, Jun. 2019.
[8] F. G. Bernard, S. Mounikaa, R. Nandhini, and A. Mohanarathinam, "Breathe analysis for identification of respiratory abnormalities using svm," in *Proc. IEEE ICACCS*, Mar. 2020, pp. 640–643.
[9] G. Benchetrit, "Breathing pattern in humans: Diversity and individuality," *Respiration Physiol.*, vol. 122, no. 2-3, pp. 123–129, Sep. 2000.
[10] C. A. K. *et al.*, "Practice parameters for the indications for polysomnography and related procedures: An update for 2005," *Sleep*, vol. 28, no. 4, pp. 499–521, 2005.
[11] Fitbit. (2014). [Online]. Available: http://www.fitbit.com
[12] Jawbone. (2014). [Online]. Available: https://jawbone.com/up
[13] F. Adib, Z. Kabelac, H. Mao, D. Katabi, and R. C. Miller, "Demo: Real-time breath monitoring using wireless signals," in *Proc. ACM MobiCom*, Sep. 2014, pp. 261–262.
[14] F. Adib, Z. Kabelac, and D. Katabi, "Multi-person localization via rf body reflections," in *Proc. USENIX NSDI*, May 2015, pp. 279–292.
[15] L. Ren, H. Wang, K. Naishadham, O. Kilic, and A. E. Fathy, "Phase-based methods for heart rate detection using uwb impulse doppler radar," *IEEE Trans. Microw. Theory Techn.*, vol. 64, no. 10, pp. 3319–3331, Oct. 2016.
[16] J. Salmi and A. Molisch, "Propagation parameter estimation, modeling and measurements for ultrawideband mimo radar," *IEEE Trans. Antennas Propag.*, vol. 59, no. 11, pp. 4257–4267, Nov. 2011.
[17] N. Patwari, L. Brewer, Q. Tate, O. Kaltiokallio, and M. Bocca, "Breathfinding: A wireless network that monitors and locates breathing in a home," *IEEE J. Sel. Topics Signal Process.*, vol. 8, no. 1, pp. 30–42, Feb. 2014.
[18] H. Abdelnasser, K. A. Harras, and M. Youssef, "Ubibreathe: A ubiquitous non-invasive wifi-based breathing estimator," in *Proc. ACM MobiHoc*, Jun. 2015, pp. 277–286.
[19] Z. Yang, P. H.Pathak, Y. Zeng, X. Liran, and P. Mohapatra, "Monitoring vital signs using millimeter wave," in *Proc. ACM MobiHoc*, Jul 2016, pp. 211–220.
[20] H. Li, X. Zeng, Y. Li, S. Zhou, and J. Wang, "Convolutional neural networks based indoor wi-fi localization with a novel kind of csi images," *China Commun.*, vol. 16, no. 9, pp. 250–260, Sep. 2019.
[21] R. M. Keenan and L. N. Tran, "Fall detection using wi-fi signals and threshold-based activity segmentation," in *Proc. IEEE PIMRC.*, Sep. 2020, pp. 1–6.
[22] H. Zou, Y. Zhou, and J. Y. et al., "Wifi-based device-free human activity recognition via automatic representation learning," in *Proc. ACM MobiCom*, vol. 17, Oct. 2017, p. 606–608.
[23] M. Z. *et al.*, "Through-wall human pose estimation using radio signals," in *Proc. IEEE CVPR*, Jun. 2018.
[24] D. Halperin, W. J. Hu, A. Sheth, and D. Wetherall, "Predictable 802.11 packet delivery from wireless channel measurements," in *Proc. ACM SIGCOMM*, Sep. 2010, pp. 159–170.
[25] Y. Xie, Z. Li, and M. Li, "Precise power delay profiling with commodity wifi," *IEEE Trans. Mobile Comput. (Early Access)*, pp. 1–1, 2018.
[26] S. Lee, Y. Park, Y. Suh, and S. Jeon, "Design and implementation of monitoring system for breathing and heart rate pattern using wifi signals," in *Proc. IEEE CCNC*, Jan. 2018, pp. 1–7.
[27] J. Zhang, Y. Hu, Y. Chen, S. M. IEEE, B. Zeng, and F. IEEE, "Breathtrack: Tracking indoor human breath status via commodity wifi," *IEEE Internet Things J.*, pp. 3899–3911, Apr. 2019.
[28] J. Liu, Y. Chen, Y. Wang, C. Xu, J. Cheng, and Y. Jie, "Monitoring vital signs and postures during sleep using wifi signals," *IEEE Internet Things J.*, vol. 5, no. 3, pp. 2071–2084, Apr. 2018.
[29] xieyaxiongfly. (2017). [Online]. Available: github.com/xieyaxiongfly
[30] J. Gjengset, J. Xiong, G. Mcphillips, and K. Jamieson, "Phaser: Enabling phased array signal processing on commodity wifi access points," in *Proc. ACM MobiCom*, Sep. 2014, pp. 153–164.
[31] S. M. M. Islam, A. Sylvester, G. Orpilla, and V. M. Lubecke, "Respiratory feature extraction for radar-based continuous identity authentication," in *Proc. IEEE RWS.*, Jan. 2020, pp. 119–122.
[32] S. K. Leem, F. Khan, and S. H. Cho, "Remote authentication using an ultra-wideband radio frequency transceiver," in *Proc. IEEE CCNC*, Jan. 2020, pp. 1–8.

Huan Dai was born in Zhenjiang, China in July 1987. He graduated with a Doctor's Degree in November 2012 and was promoted to Associate Professor in July 2015. He joined Suzhou University of Science and Technology in February 2017. From March 2019 to January 2021, he was seconded to the Development Center of Degree and Postgraduate Education of the Ministry of Education.

The main research directions are Internet of things technology, wireless sensing technology, indoor positioning technology and signal processing. He has published more than 40 academic papers, of which more than 20 are included in SCI and EI, cited more than 60 times, applied for 8 invention patents, 4 authorized patents and 6 software copyrights.

Jingjing Jiang was born in September 1995 in Lianyungang, Jiangsu Province, China, graduated from Suzhou University of Science and Technology. Now she is a Graduate Student in the School of Electronics and Information of Suzhou University of Science and Technology. The research direction is wireless sensing, indoor positioning, signal processing. Published a Chinese Journal paper.

Jiaju Ma was born in Suzhou, China in January 1999. He is currently studying for a Master's Degree at Suzhou University of Science and Technology. The main research direction is wireless perception. Engaged in the research of breathing recognition and heartbeat recognition based on channel state information.

He Huang , male, Professor, Doctor, Doctoral Supervisor, Deputy Director of Embedded Bionic Intelligence Research Institute of Suzhou University. ACM, IEEE, CCF, member of China Electronics Society, Member of Internet of Things Special Committee of China Computer Society (CCF) since 2012. The third level training object of "333 project" in Jiangsu Province is the 2019 annual education figure nomination award of Jiangsu Province (only 10 people in the whole province and 1 person in the University).

In June 2011, he graduated from the Software and Theory Direction of School of Computer Science and Technology of China University of Science and Technology with a Doctor's Degree in Engineering. He studied with academician Chen Guoliang and joined Suzhou University in August of the same year. He was promoted to Associate Professor in 2013 and Professor in August 2018. From January 2019 to January 2020, he is engaged in cooperative research at the University of Florida, public Ivy League. In recent years, the specific research directions include information security and privacy protection, traffic statistics, group intelligence perception computing, software defined network, traffic big data, etc.

Hongbo Liu joined the School of Computer Science and Engineering (School of Cybersecurity) at University of Electronic Science and Technology of China since 2020. Before that he was an Associate Professor in the Department of Computer Information and Technology at Indiana University-Purdue University Indianapolis (IUPUI), USA. He obtained his Ph.D. degree from the Department of Electrical and Computer Engineering at Stevens Institute of Technology under the supervision. He had both his Master and Bachelor Degree from University of Electronic Science and Technology of China in 2008 and 2005, respectively. He has published over 60 journal articles and referred conference papers, including ACM MobiCom, IEEE TMC, IEEE INFOCOM, etc. He is also the Recipient of the Best Paper Award from ACM MobiCom 2011, Best Paper Runner-up Award from IEEE CNS 2013, and Best Paper Award from IEEE CNS 2018.